ADVANCED MATERIALS
www.advmat.de

Materials Views
www.MaterialsViews.com

Atomic Layer Deposited Gallium Oxide Buffer Layer Enables 1.2 V Open-Circuit Voltage in Cuprous Oxide Solar Cells

Yun Seog Lee, Danny Chua, Riley E. Brandt, Sin Cheng Siah, Jian V. Li, Jonathan P. Mailoa, Sang Woon Lee, Roy G. Gordon, and Tonio Buonassisi**

With the growing demand for low-cost solar cells that are truly scalable to the terawatts level, Earth-abundant and air-stable semiconductor materials are considered a promising candidate class of materials.[1–3] Cuprous oxide (Cu_2O) is an Earth-abundant semiconductor with over 20% single-junction theoretical maximum power conversion efficiency (PCE).[4] In particular, its large bandgap (E_g) of ~2 eV is suitable for a top-cell in a tandem device with conventional silicon- or CIGS-based solar cells.[5] Due to the intrinsic *p*-type conductivity of this material, creating a *p*–*n* homojunction of Cu_2O has been considered challenging.[6,7] Instead, the most effective approach to fabricate Cu_2O-based solar cells has been a heterojunction device architecture with an *n*-type transparent conducting oxide (TCO) including zinc oxide (ZnO) and indium tin oxide.[8–11] However, the PCEs of Cu_2O-based heterojunction devices have remained low, largely due to staggered gap (type-II heterojunction) electronic band alignment with the TCO layers as well as a high density of defects at the heterojunction interface.[8,12] The type-II heterojunction creates an effective energy gap for interface recombination ($E_{g,IF}$) smaller than the E_g of Cu_2O, resulting in a higher interface recombination rate and a significantly reduced open-circuit voltage (V_{OC}).[13]

To mitigate the non-ideal heterojunction, various buffer layers have been inserted between the Cu_2O and TCO layers.[8,9,14] Properly controlled electronic band alignment of the buffer layer and defect density at the interface region has enhanced the device performance significantly. So far, a gallium oxide (Ga_2O_3) buffer layer grown by pulsed laser deposition technique has shown the highest PCE of 5.38% among Cu_2O-based solar cells with a V_{OC} of 0.8 V.[9] Ga_2O_3 is a wide-bandgap semiconductor ($E_g \approx 5$ eV) that has been studied for UV-transmitting optoelectronic applications, demonstrating surface-defect passivation properties.[15,16] While theoretical and experimental studies showed *n*-type conductivity of this material, undoped Ga_2O_3 thin-films often behave like an insulator due to the large bandgap.[17,18] For solar cell applications, undoped Ga_2O_3 has been used as an insulating layer in conductor-insulator-semiconductor type solar cells and dye-sensitized solar cells.[19–21] In those solar cell applications, the Ga_2O_3 layer was sufficiently thin (less than ~2 nm) to allow a tunneling current. In Cu_2O-based solar cells, on the other hand, a Ga_2O_3 layer up to 90 nm did not obstruct photo-current, which suggests that the electronic band of the Ga_2O_3 layer is favorably aligned with neighboring layers, Cu_2O and aluminum-doped zinc oxide (ZnO:Al).[22]

In this communication, we demonstrate Cu_2O-based heterojunction thin-film solar cells with a higher V_{OC} by incorporating an atomic layer deposited Ga_2O_3 buffer layer. The atomic layer deposition (ALD) technique is increasingly applied for photovoltaic applications, in particular for depositing buffer layers and surface passivation layers.[23,24] On an electrochemically-deposited Cu_2O layer, we deposit a 10-nm-thick Ga_2O_3 buffer layer that reduces interfacial recombination by improving band-alignment across the heterojunction and reducing the interface defect density. The band-alignment of the Ga_2O_3 layer is characterized by X-ray photoelectron spectroscopy (XPS) and optical measurements. The Ga_2O_3 buffer layer shows an improved conduction-band offset relative to the Cu_2O layer, compared with that of other buffer layers reported previously. Also, the XPS measurements reveal that the ALD conditions for the buffer layer growth reduce the density of Cu^{2+}-related defects at the Ga_2O_3/Cu_2O interface. Using Ga_2O_3 buffer layers, we fabricate Cu_2O-based thin-film solar cells, demonstrating a National Renewable Energy Laboratory (NREL)-certified PCE and V_{OC} of 3.97% and 1.20 V, respectively; a pseudo-efficiency of 7.2% was obtained by J_{SC}-V_{OC} measurements, which removes the effects of series resistance.[25,26] The device characteristics are further investigated by temperature-dependent current density vs. voltage (*J*–*V*) and bias-dependent external quantum efficiency (EQE) measurements to elucidate the performance-loss mechanisms in these devices.

Ga_2O_3 thin-films were deposited at 120 °C in a custom-built cylindrical ALD reactor with a sample stage 30 cm long and 3 cm wide, and a chamber volume of 0.627 L. Bis(μ-dimethylamino)tetrakis(dimethylamino)digallium (**Figure 1**a) and H_2O were used as a gallium precursor and an oxygen source, respectively.[27] During the ALD process of Ga_2O_3 films,

Dr. Y. S. Lee,[+] R. E. Brandt, S. C. Siah, J. P. Mailoa, Prof. T. Buonassisi
Massachusetts Institute of Technology
Cambridge, Massachusetts 02139, USA
E-mail: buonassisi@mit.edu
D. Chua,[+] Dr. S. W. Lee, Prof. R. G. Gordon
Department of Chemistry and Chemical Biology
Harvard University
Cambridge, Massachusetts 02138, USA
E-mail: gordon@chemistry.harvard.edu
Dr. J. V. Li
National Renewable Energy Laboratory
Golden, Colorado 80401, USA
[+]These authors contributed equally to this work.

DOI: 10.1002/adma.201401054

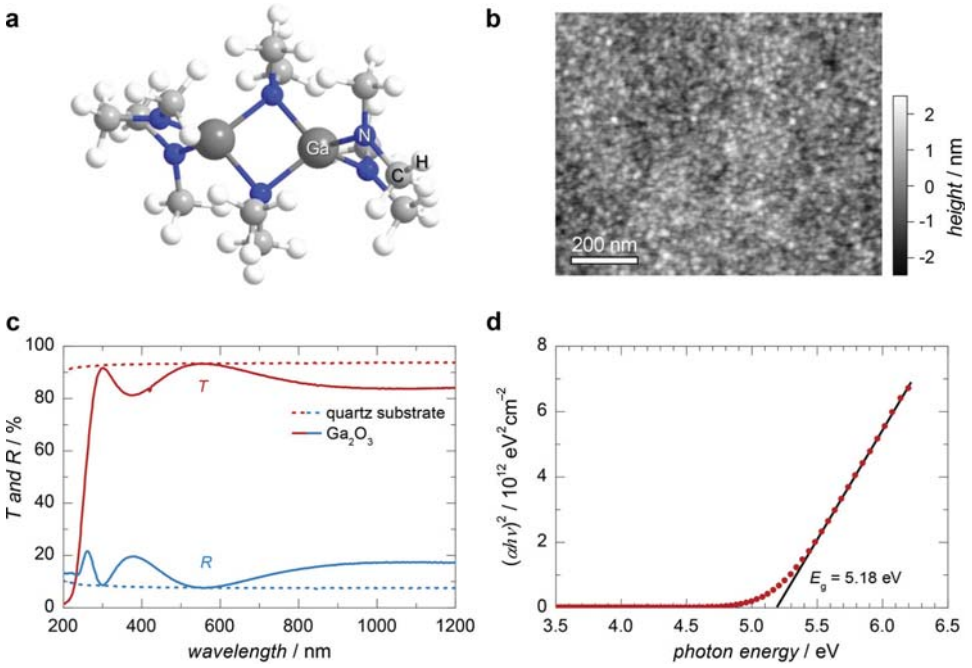

Figure 1. (a) The molecular structure of the ALD Ga precursor, bis(μ-dimethylamino)tetrakis(dimethylamino)digallium. (b) The surface morphology of a Ga_2O_3 film deposited on a Si wafer measured by AFM. (c) The optical transmission (*T*) and reflection (*R*) spectra of a 0.2-μm-thick Ga_2O_3 film on a UV-grade quartz substrate. (d) Bandgap estimation of the ALD Ga_2O_3 film by a linear extrapolation.

the temperatures of the gallium precursor and oxygen source were maintained at 107 and 25 °C, respectively. High-purity N_2 was used as a carrier gas. The exposures of the gallium precursor and H_2O were estimated to be approximately 3 and 5 Torr·s, respectively. The deposition rate was measured to be ~0.2 nm per cycle. The atomic ratio between Ga and O in the deposited film was measured by Rutherford backscattering spectrometry (RBS). Figure S1 shows the RBS spectrum of a Ga_2O_3 film deposited on a glassy carbon substrate, which indicates a near stoichiometric ratio of Ga:O of 1:1.6. We investigate the microstructure of the Ga_2O_3 film using atomic force microscopy (AFM) and X-ray diffraction (XRD) measurements. The AFM image in Figure 1b shows a smooth surface morphology of a 50-nm-thick Ga_2O_3 film with a grain size range of 10 – 20 nm and a root mean square roughness value of ~0.3 nm. The XRD spectrum shown in Figure S2 exhibits no specific peaks from the film, which suggests near amorphous or nano-crystalline structure of the film. The film is too electrically insulating to measure the resistivity.

To estimate the optical bandgap of the Ga_2O_3 films, we measured the optical transmission and reflection spectra of Ga_2O_3 films by using a UV-VIS-IR spectrophotometer. As shown in Figure 1c, a 200-nm-thick Ga_2O_3 film deposited on a UV-grade quartz substrate showed excellent optical transmission over a wavelength range down to ~300 nm. The film's optical bandgap is estimated by a linear extrapolation using the relation of $(\alpha h\nu)^2 \propto (h\nu - E_g)$, where α, h, and ν are the optical absorption coefficient, Planck constant, and photon frequency, respectively. The band gap of the Ga_2O_3 film was estimated to be 5.18 eV, which is slightly larger than the values (4.9 – 5.0 eV) reported previously.[16,28]

Using the optical bandgap, the electronic band alignment of the Ga_2O_3 relative to Cu_2O is investigated by X-ray photoelectron spectroscopy (XPS), following the procedure by Waldrop *et al.* (Figure S3 and S4).[29] The binding energies of Cu-2*p* and Ga-2*p* core levels ($E_{Cu-2p}^{Cu_2O}$ and $E_{Ga-2p}^{Ga_2O_3}$) with respect to valence band edge positions of Cu_2O and Ga_2O_3 bulk films ($E_{VBM}^{Cu_2O}$ and $E_{VBM}^{Ga_2O_3}$) are measured to be 932.47 ± 0.04 and 1114.46 ± 0.15 eV, respectively.[8] We also prepared a stack sample which consists of a ~1-nm-thick Ga_2O_3 layer grown by ALD on an electrochemically deposited ~2.5-μm-thick Cu_2O film grown following the procedure described in previous studies.[8,30] The Ga_2O_3 overlayer is sufficiently thin to measure the binding energies of Cu and Ga core levels simultaneously from the sample. The relative energy difference of –185.26 eV between the two core levels ($E_{Cu-2p}^{Ga_2O_3/Cu_2O} - E_{Ga-2p}^{Ga_2O_3/Cu_2O}$) were used to calculate the conduction band offset in the Ga_2O_3/Cu_2O stack sample (ΔE_{CB}) by the relation

$$\Delta E_{CB} = \left(E_{Cu-2p}^{Ga_2O_3/Cu_2O} - E_{Ga-2p}^{Ga_2O_3/Cu_2O}\right) + \left(E_{Ga-2p}^{Ga_2O_3} - E_{VBM}^{Ga_2O_3}\right) - \left(E_{Cu-2p}^{Cu_2O} - E_{VBM}^{Cu_2O}\right) + \left(E_g^{Ga_2O_3} - E_g^{Cu_2O}\right) \quad (1)$$

where $E_g^{Ga_2O_3}$ and $E_g^{Cu_2O}$ are the bandgap of the bulk Ga_2O_3 (5.18 eV) and Cu_2O (2.09 eV), respectively.[31] The ΔE_{CB} is determined to be –0.18 ± 0.16 eV (cliff) with a valence band offset of –3.27 ± 0.16 eV, indicating a type-II heterojunction where the interface recombination takes place between holes from Cu_2O and electrons from Ga_2O_3. As depicted in **Figure 2**a, the effective energy gap for interface recombination ($E_{g,IF}$) in the heterojunction is 1.91 ± 0.16 eV which is the energy level difference between the valence band edge of Cu_2O and the conduction band edge of Ga_2O_3.[13]

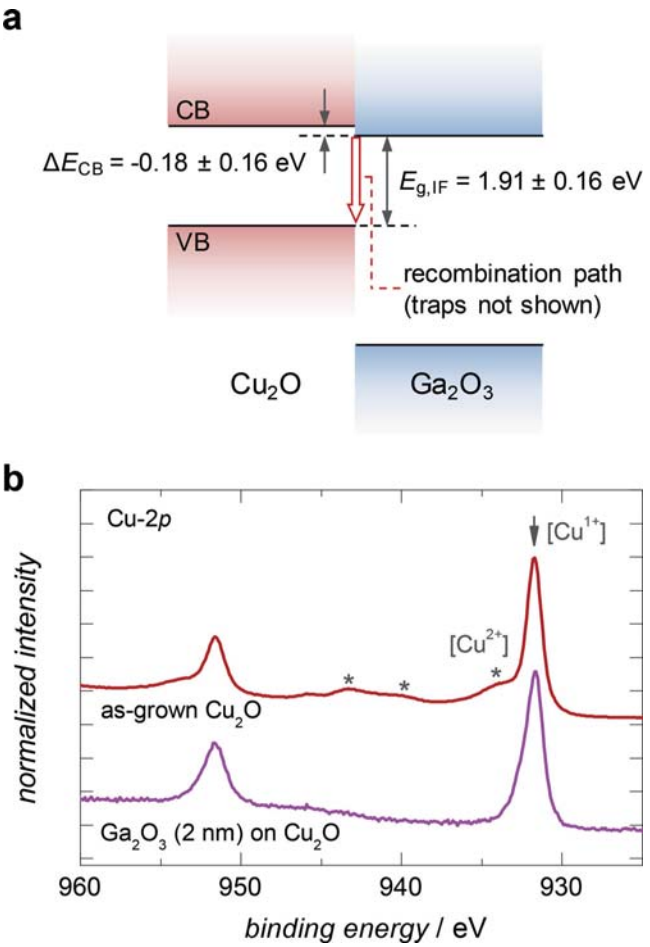

Figure 2. (a) The electronic band alignment of the Ga_2O_3/Cu_2O heterojunction derived from XPS and optical bandgap measurements, showing a type-II heterojunction with a ΔE_{CB} of −0.18 ± 0.2 eV. (b) The XPS spectra of the Cu-2*p* core level for an as-grown Cu_2O sample and a Ga_2O_3 (2 nm) / Cu_2O stack sample, which shows a reduction of the Cu^{2+}-related peaks (asterisks) by the Ga_2O_3 overlayer.

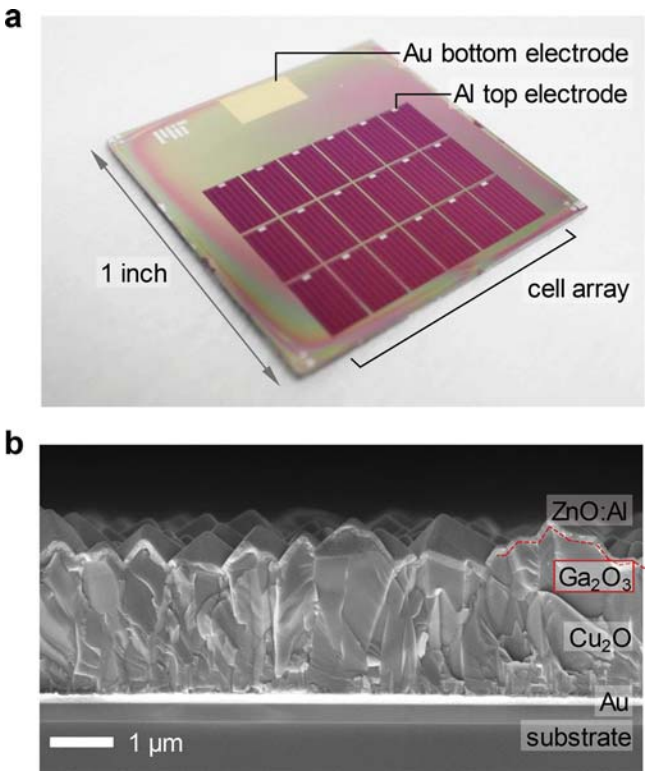

Figure 3. (a) A photograph of the fabricated Cu_2O-based thin-film solar cell device, showing a 3 × 6 array of fully-isolated 3 mm × 5 mm size cells. (b) A cross-sectional SEM image of the device, showing the device structure of ZnO:Al (80 nm)/Ga_2O_3 (10 nm)/Cu_2O (~2.5 μm)/Au (200 nm) on a SiO_2 (0.3 μm)/Si substrate. The red dashed line indicates the ALD Ga_2O_3 buffer layer.

In addition, the chemical state of Cu at the interface is identified by XPS to investigate the defect density at the Ga_2O_3/Cu_2O interface. The Cu^{2+}-related state at the interface has been considered to create deleterious traps that promote interface recombination.[30,32] Figure 2b shows the XPS spectra of the Cu-2*p* core levels of the Ga_2O_3/Cu_2O stack sample and an as-grown Cu_2O bulk sample. The bulk Cu_2O sample shows two main peaks at 932.3 and 952 eV corresponding to the $2p_{3/2}$ and $2p_{1/2}$ levels of Cu^{1+} state (Cu_2O). A shoulder peak at 934.0 eV and broad satellite peaks at the 940 – 945 eV region can be also observed, both of which were attributed to the presence of the Cu^{2+} state (CuO) on the surface.[33] A ~1 nm CuO surface layer is normally formed by an air exposure after electrochemical deposition of Cu_2O. On the other hand, the Ga_2O_3/Cu_2O stack sample does not show the shoulder peak and satellite peaks from CuO, but two peaks of Cu^{1+} only. Similar reduction behavior of CuO to Cu_2O by diethylzinc as a Zn ALD precursor has been reported previously, which reduced the density of Cu^{2+}-related defect at interface and improved the device performance.[30] The change of Cu-2*p* spectra suggests that the gallium precursor passivates the Cu^{2+}-related interface defect effectively during the Ga_2O_3 ALD process, by reducing the CuO surface layer to Cu_2O.

To demonstrate the effect of the Ga_2O_3 buffer layer on Cu_2O-based solar cell performance, we fabricated Cu_2O-based thin-film solar cells by incorporating a 10-nm-thick Ga_2O_3 layer. **Figure 3** shows a cross-sectional scanning electron microscopy (SEM) image and a schematic structure of the device: ZnO:Al *n*-type TCO (thickness: 80 nm)/Ga_2O_3 buffer (10 nm)/Cu_2O *p*-type absorber (2.5 μm)/Au bottom electrode (200 nm). Due to the (111)-preferred growth orientation of polycrystalline Cu_2O thin-films by the electrochemical deposition condition, the morphology of the Cu_2O layer shows a rough surface texture that reduces optical reflection. The ZnO:Al and Ga_2O_3 layers were deposited conformally on the rough surface of Cu_2O by ALD at 120 °C. The same ALD chamber was used, without breaking vacuum, to create a clean interface between ZnO:Al and Ga_2O_3. The devices were completed by depositing an Al top-electrode grid (1 μm) and a MgF_2 anti-reflective layer (95 nm). The optimal thickness of the MgF_2 layer was determined by optical simulation using a finite-difference time-domain (FDTD) optical simulation using the FDTD Solutions software (Lumerical Solutions, Inc.) to enhance optical absorption of the device.

The photovoltaic performance of a device was characterized independently at the NREL and in-house (Table S1). The *J–V*

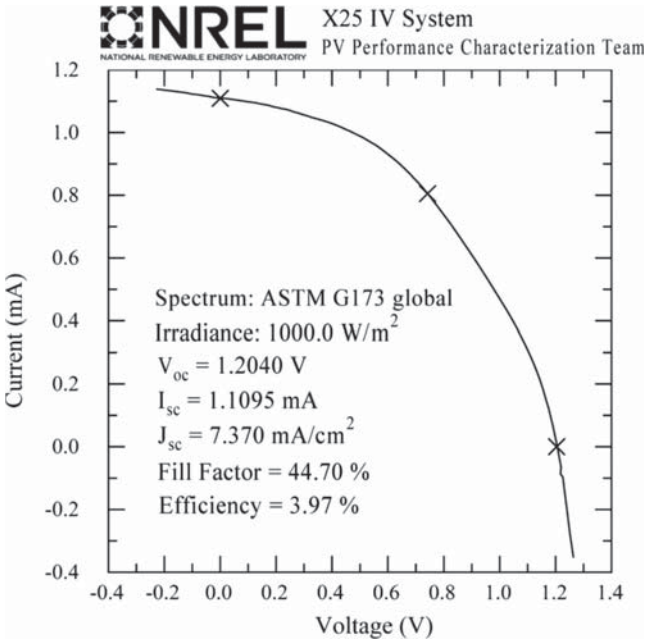

Figure 4. The *J–V* curve and photovoltaic characteristics under AM1.5 global normal spectral irradiance (ASTM G173, IEC 60904–3 edition 2 at 25 °C), measured at NREL.

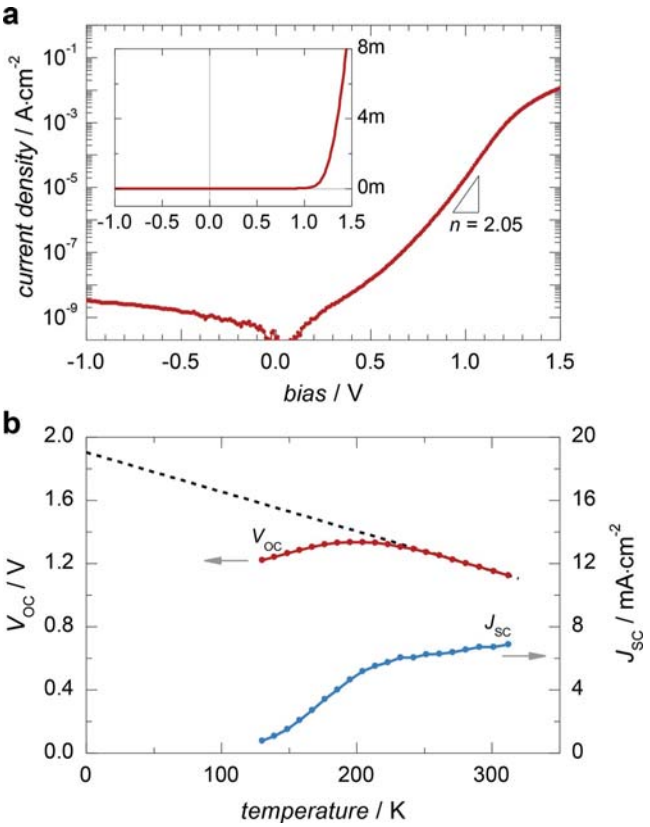

Figure 5. (a) *J–V* characteristics of the device under a dark condition in a semi-log scale and a linear scale (inset). The slope of the semi-log scale plot shows an ideality factor of ~2.05 near a bias condition of 1 V. (b) Temperature-dependence of the V_{OC} and J_{SC} of the device under a ~0.9-sun illumination condition. The dotted line indicates a linear extrapolation of the V_{OC} to a temperature of 0 K.

characteristic of the device under 1-Sun AM1.5 global normal spectral irradiance (ASTM G173, IEC 60904–3 edition 2 at 25 °C) is shown in **Figure 4**. The device was placed on a temperature-controlled stage to maintain the device temperature at 24.6 ± 0.5 °C. A spectral mismatch correction was also applied using an EQE spectrum with a light bias of 0.4 mA by a white light-emitting-diode to measure accurate device performance, as shown in Figure S5. The device exhibits a PCE of 3.97%. The V_{OC}, the short circuit current density (J_{SC}), and fill-factor (FF) of the device are 1.20 V, 7.37 mA·cm^{-2}, and 44.7%, respectively. The low FF originates from the high series-resistance of the device and reduced photo-generated carrier collection efficiency at increased forward bias condition. Since the TCO and electrodes are designed to have a series resistance smaller than 0.7 Ω·cm^2, the resistance from Cu_2O and Ga_2O_3 layers could be a major contribution to the series resistance of the device. An implied *J–V* curve is characterized by J_{SC}–V_{OC} measurements under a steady-state illumination, as shown in Figure S6. The implied *J–V* curve indicates that the FF can be improved up to 84% if the non-idealities are eliminated, which would yield a device with a pseudo-PCE of 7.2%.[25,26] The V_{OC} in this study represents a significant improvement over previously reported state-of-the-art Cu_2O-based devices, including the Cu_2O/GaN (V_{OC} = 0.85 V) and Cu_2O/CH_3CN liquid junction (0.82 V) devices as well as the device with a Ga_2O_3 buffer layer grown by pulsed laser deposition (0.8 V).[4,9,34] This breakthrough is made possible by improved band-alignment and reduced interface-defects by the ALD-Ga_2O_3 layer. However, the measured V_{OC} is still lower than the expected limit (~1.7 V) proposed by King et al., which can be attained when only radiative recombination occurs in Cu_2O.[35]

To investigate the dominant recombination process in the device, *J–V* characteristics of the device were also measured under a dark condition. **Figure 5**a shows a semi-log scale and linear scale plot of *J–V* of a 3 × 5 mm^2 size device at room temperature. The *J–V* plot shows a rectifying curve that can be modeled by using the Shockley's diode equation

$$J = J_0\left(\exp\left(\frac{qV}{nkT}\right)-1\right) \quad (2)$$

where J_0, q, n, k, and T are the saturation current density, electron charge, diode ideality factor, Boltzmann constant, and temperature of the device. Since the *J–V* characteristics near zero bias and high forward-bias regions are affected by a shunt resistance and a series resistance, respectively, we fit the measured *J–V* curve near 1.0 V bias to Equation (2). The fitted parameters of J_0 and n are estimated to be 1.8 × 10^{-13} A·cm^{-2} and 2.05, respectively. The ideality factor near 2 indicates that Shockley-Read-Hall (SRH) recombination occurs primarily in the space charge region (SCR). In the case that J_0 is driven by SRH recombination in the SCR of the Cu_2O layer only, the associated ideal J_0 is expected to be on the order of 10^{-17} – 10^{-18} A·cm^{-2} for Cu_2O by the relation $J_0 \approx \exp\left(-E_g/2kT\right)$.[36] If the dominating SRH recombination is assumed to occur at the Cu_2O/Ga_2O_3 interface, the relation provides a range of J_0 in the order of 10^{-15} – 10^{-18} A·cm^{-2} by using the $E_{g,IF}$ of

1.91 ± 0.16 eV. The fitted J_0 being higher than the ideal values suggests that an additional pre-factor (J_{00}) should be involved in the description of J_0 to explain the recombination in the polycrystalline and non-epitaxial heterojunction device, which typically contains a high density of interface defects.

The origin of recombination in the device is further analyzed by a temperature-dependent J–V measurement under an illuminated condition. The device was placed in the cryostat under vacuum, illuminated with a solar simulator and a set of neutral density filters to achieve ~0.9-sun light intensity. To determine the activation energy (E_A) of J_0, we plot V_{OC} and J_{SC} as a function of device temperature from 130 to 312 K, as shown in Figure 5b. The temperature-dependence of V_{OC} can be modeled as

$$V_{OC} = \frac{E_A}{q} - \frac{nkT}{q}\ln\left(\frac{J_{00}}{J_{SC}}\right) \quad (3)$$

where J_{00} is the temperature-independent pre-factor of J_0 in the relation of $J_0 = J_{00}\exp(-E_A/nkT)$.[37] If the n, J_{SC}, and J_{00} are independent of T, an extrapolation of V_{OC} to $T = 0$ K indicates the E_A of the J_0. Due to a high carrier-activation energy (0.16 – 0.42 eV) of Cu_2O, a significant carrier freeze-out occurs in the Cu_2O layer as temperature decreases, resulting in a higher resistance.[38] In the low-temperature regime, the photovoltaic performance is reduced significantly, possibly because the device becomes highly resistive. The linear portion of V_{OC} at a temperature range between 270 and 312 K is used for the extrapolation. The extrapolated E_A is approximately 1.9 eV, which is consistent with the $E_{g,IF}$ measured by the XPS and optical bandgap. The estimated E_A suggests that the dominating recombination in the devices occurs at the Cu_2O/Ga_2O_3 interface. The fitted value of J_0 being higher than the ideal case can be attributed largely to the J_{00}, which can be a measure of the heterojunction interface quality.[13] To further enhance the V_{OC} of the Cu_2O/Ga_2O_3 devices, a lower J_{00} and a higher J_{SC} are desired, which can be achieved by reducing the density of interface recombination centers and enhancing the collection efficiency of photo-generated carriers, respectively.

The collection efficiency of photo-generated carriers by the device is investigated by bias-dependent EQE measurements. **Figure 6**a shows EQE spectra of the device in the wavelength range between 300 and 700 nm under various bias conditions (–0.8, –0.4, 0, 0.4, and 0.8 V) and the absorption depth (α^{-1}) calculated from the α of Cu_2O.[31] At zero bias, the spectrum shows EQE higher than 90% over a wavelength range between 390 and 480 nm. On the other hand, the EQE drops significantly for the long wavelength range (>480 nm) where the photons are absorbed far from the heterojunction interface. The low EQE in the long wavelength range originates from the limited drift- and diffusion-lengths of photo-generated carriers of electrochemically deposited Cu_2O thin films.[8,39,40] Figure 6b shows the change of EQE under biased conditions relative to the zero-bias condition. The change of the EQE occurs predominantly in the long wavelength range, which indicates that the photo-generated carrier collection relies considerably on drift in the depletion region. At a forward bias of 0.8 V which is near the maximum power condition, the decreased drift length as well as the series resistance reduce the EQE significantly. Compared to the short-circuit condition, forward bias reduces the electric field assisting carrier drift due to the flatter band bending near the junction. Figure 6c shows the simulated optical absorption spectra of each layer in the device, calculated by the FDTD optical simulation. The simulated absorption spectrum of the Cu_2O layer shows a J_{SC} entitlement of 11.5 mA·cm^{-2} with the current device geometry, compared to a theoretical entitlement of ~15 mA·cm^{-2}.[11] The bias-dependent EQE and the simulated optical absorption spectrum of Cu_2O suggest that the FF and J_{SC} of the device can be further enhanced by improving the minority carrier diffusion length in Cu_2O.

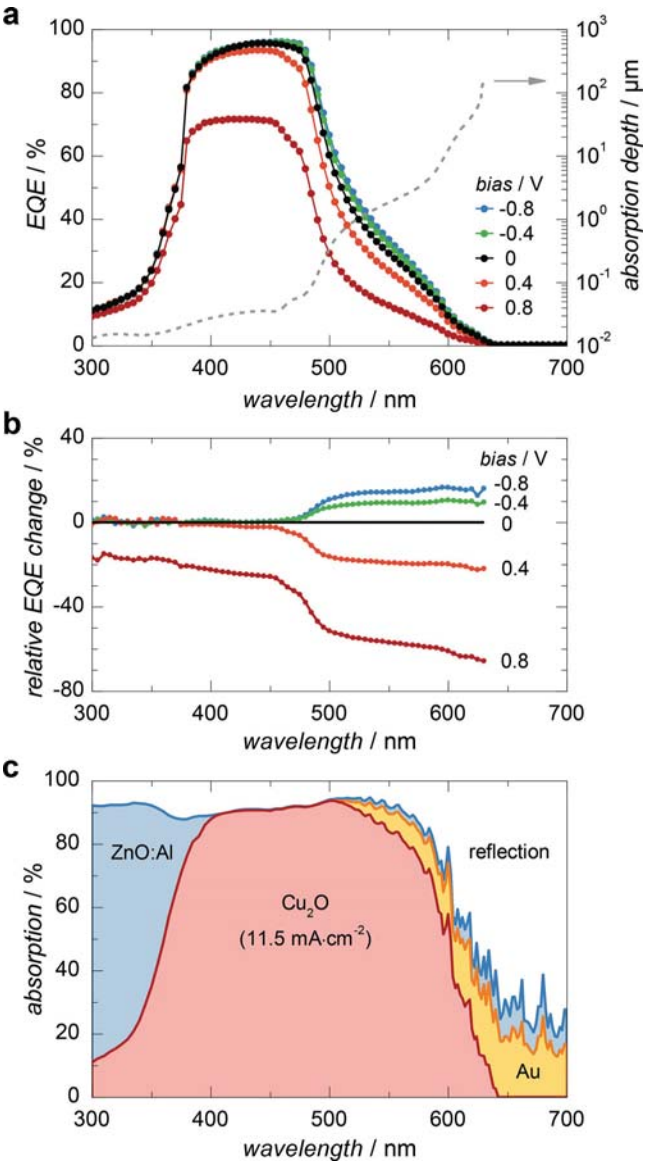

Figure 6. (a) The spectra of bias-dependent EQE of the device and calculated absorption depth (α^{-1}) of Cu_2O. (b) The change of EQE under various bias conditions relative to a zero bias condition. (c) Calculated optical absorption spectra of each layer in the device by the FDTD optical simulation, indicating a J_{SC} entitlement of 11.5 mA·cm^{-2}. The simulation shows a negligible optical loss by the Ga_2O_3 layer. The achieved J_{SC} (7.37 mA·cm^{-2}) suggests this device is not optically limited, but instead limited by poor carrier collection.

In conclusion, we have successfully demonstrated that atomic layer deposited Ga_2O_3 is a highly suitable buffer layer for enhancing the PCE and V_{OC} of Cu_2O-based solar cells. Pairing Cu_2O with a 10-nm-thick Ga_2O_3 layer provides a near ideal conduction band offset, reducing interface recombination. The gallium ALD precursor provides an effective reduction of Cu^{2+}-related defects at heterojunction interface as well as a highly conformal deposition of the buffer layer on the rough Cu_2O surface. NREL certified the PCE of a device with a Ga_2O_3 buffer layer to be 3.97% with a V_{OC} of 1.20 V at a temperature of 24.6 ± 0.5 °C. The temperature-dependent *J–V* characteristics of the device indicate that the dominant recombination process occurs near the Ga_2O_3/Cu_2O interface. The EQE spectra also show that the device performance is still limited significantly by inefficient photo-generated carrier collection in addition to the high series resistance; enhancement of carrier collection length and complete removal of series resistance are estimated to enable device efficiencies approaching 11.5% (V_{OC} = 1.20 V, J_{SC} = 11.5 mA·cm^{-2}, and FF = 84%).

Experimental Section

Solar Cell Fabrication: A silicon wafer with a 0.3-μm-thick thermal oxide (SiO_2) surface layer was diced into 1 × 1 inch^2 sized pieces to be used for substrates. A stack of Ti (5 nm)/Au (200 nm)/Ti (5 nm) layers was deposited by e-beam evaporation, followed by a deposition of a 2.5-μm-thick SiO_2 layer by plasma-enhanced chemical vapor deposition. To define a 3 × 6 cell array with a cell area of 3 × 5 mm^2, the SiO_2/Ti layers were etched selectively by photolithography and buffered-oxide-etchant (7:1, J. T. Baker), exposing the Au layer. A 2.5-μm-thick Cu_2O film was deposited on the exposed Au area by the galvanostatic electrochemical method at 40 °C, as described in detail elsewhere.[8,41] A 10-nm-thick Ga_2O_3 buffer layer and a 80-nm-thick ZnO:Al TCO layer were deposited by ALD on the entire area of the substrate. The ZnO:Al layer was deposited using trimethylaluminum, diethylzinc, and de-ionized water as Al, Zn, and O sources, respectively. A trimethylaluminum pulse was introduced after every set of 19 pulses of diethylzinc to reduce the sheet resistance of the ZnO:Al layer down to ~1 kOhm·sq^{-1}. 1-μm-thick Al top-electrodes were deposited by e-beam evaporation with grid spacing of 0.5 mm defined by a lift-off process. To isolate cells, the Ga_2O_3 and ZnO:Al layers were wet-etched partially by a photolithography process. A 95-nm-thick MgF_2 film as an anti-reflective layer was deposited by thermal evaporation.

Characterization: Surface morphologies were probed by atomic force microscopy using MFP-3D SA (Asylum Research). The microstructures of the Ga_2O_3 films were characterized by XRD using a PANalytical X'Pert Pro diffractometer with Cu-*Kα* radiation. Surface morphologies of the devices were analyzed using an Ultra 55 FESEM (Zeiss). XPS measurements were performed by using a PHI VersaProbe II (Physical Electronics) and a K-alpha XPS (Thermo Scientific). The optical properties of the Ga_2O_3 films were measured by using a Lambda 950 UV-VIS-NIR spectrophotometer (PerkinElmer) equipped with an integrating sphere, and by a V-VASE32 spectroscopic ellipsometer (J. A. Woollam Co.). The *J–V* characteristics of the devices were measured by using a Keithley 2400 sourcemeter. The EQE of the device was measured by using a QEX7 (PV Measurements) calibrated with a NIST-certified Si photodiode.

Supporting Information

Supporting Information is available from the Wiley Online Library or from the author.

Acknowledgements

We thank P. Ciszek and K. Emery (NREL) and their team for the certified cell testing. We also thank Prof. J. Heo (Chonnam National Univ., Korea), K. Hartman, and K. Broderick (MIT) for helpful discussions and experimental support. This work was supported by the National Science Foundation (NSF) award CBET-1032955, NSF CAREER award ECCS-1150878, and the NREL as a part of the Non-Proprietary Partnering Program under Contract No. De-AC36–08-GO28308 with the U.S. Department of Energy. This work made use of the Microsystems Technology Laboratories at MIT and the Center for Nanoscale Systems at Harvard University supported by NSF awards DMR-0819762 and ECS-0335765, respectively. An NSF Graduate Research Fellowship (R.E.B.) and a Clean Energy Scholarship from NRF Singapore (S.C.S.) are acknowledged.

Received: March 6, 2014
Revised: April 10, 2014
Published online:May 23, 2014

[1] A. Shah, P. Torres, R. Tscharner, N. Wyrsch, H. Keppner, *Science* **1999**, *285*, 692.
[2] C. Wadia, A. P. Alivisatos, D. M. Kammen, *Environ. Sci. Technol.* **2009**, *43*, 2072.
[3] S. Rühle, A. Y. Anderson, H.-N. Barad, B. Kupfer, Y. Bouhadana, E. Rosh-Hodesh, A. Zaban, *J. Phys. Chem. Lett.* **2012**, *3*, 3755.
[4] B. K. Meyer, A. Polity, D. Reppin, M. Becker, P. Hering, P. J. Klar, T. Sander, C. Reindl, J. Benz, M. Eickhoff, C. Heiliger, M. Heinemann, J. Bläsing, A. Krost, S. Shokovets, C. Müller, C. Ronning, *Phys. Status Solidi B* **2012**, *249*, 1487.
[5] Z. M. Beiley, M. D. McGehee, *Energy Environ. Sci.* **2012**, *5*, 9173.
[6] J. Robertson, S. J. Clark, *Phys. Rev. B* **2011**, *83*, 075205.
[7] D. O. Scanlon, G. W. Watson, *J. Phys. Chem. Lett.* **2010**, *1*, 2582.
[8] Y. S. Lee, J. Heo, S. C. Siah, J. P. Mailoa, R. E. Brandt, S. B. Kim, R. G. Gordon, T. Buonassisi, *Energy Environ. Sci.* **2013**, *6*, 2112.
[9] T. Minami, Y. Nishi, T. Miyata, *Appl. Phys. Express* **2013**, *6*, 044101.
[10] A. Mittiga, E. Salza, F. Sarto, M. Tucci, R. Vasanthi, *Appl. Phys. Lett.* **2006**, *88*, 163502.
[11] K. P. Musselman, A. Wisnet, D. C. Iza, H. C. Hesse, C. Scheu, J. L. MacManus-Driscoll, L. Schmidt-Mende, *Adv. Mater.* **2010**, *22*, E254.
[12] K. P. Musselman, A. Marin, A. Wisnet, C. Scheu, J. L. MacManus-Driscoll, L. Schmidt-Mende, *Adv. Funct. Mater.* **2011**, *21*, 573.
[13] R. Scheer, *J. Appl. Phys.* **2009**, *105*, 104505.
[14] Z. Duan, A. Du Pasquier, Y. Lu, Y. Xu, E. Garfunkel, *Sol. Energy Mater. Sol. Cells* **2012**, *96*, 292.
[15] C. A. Lin, H. C. Chiu, T. H. Chiang, T. D. Lin, Y. H. Chang, W. H. Chang, Y. C. Chang, W.-E. Wang, J. Dekoster, T. Y. Hoffmann, M. Hong, J. Kwo, *Appl. Phys. Lett.* **2011**, *98*, 062108.
[16] M. Orita, H. Ohta, M. Hirano, H. Hosono, *Appl. Phys. Lett.* **2000**, *77*, 4166.
[17] N. Ueda, H. Hosono, R. Waseda, H. Kawazoe, *Appl. Phys. Lett.* **1997**, *70*, 3561.
[18] J. B. Varley, J. R. Weber, A. Janotti, C. G. Van de Walle, *Appl. Phys. Lett.* **2010**, *97*, 142106.
[19] A. K. Chandiran, M. K. Nazeeruddin, M. Grätzel, *Adv. Funct. Mater.* **2014**, *24*, 1615.
[20] A. K. Chandiran, N. Tetreault, R. Humphry-Baker, F. Kessler, E. Baranoff, C. Yi, M. K. Nazeeruddin, M. Grätzel, *Nano Lett.* **2012**, *12*, 3941.
[21] R. Singh, M. A. Green, K. Rajkanan, *Sol. Cells* **1981**, *3*, 95.
[22] T. Minami, Y. Nishi, T. Miyata, *Thin Solid Films* **2013**, *549*, 65.
[23] J. R. Bakke, K. L. Pickrahn, T. P. Brennan, S. F. Bent, *Nanoscale* **2011**, *3*, 3482.

[24] P. Poodt, A. Lankhorst, F. Roozeboom, K. Spee, D. Maas, A. Vermeer, *Adv. Mater.* **2010**, *22*, 3564.
[25] M. J. Kerr, A. Cuevas, R. A. Sinton, *J. Appl. Phys.* **2002**, *91*, 399.
[26] M. Wolf, H. Rauschenbach, *Adv. Energy Convers.* **1963**, *3*, 455.
[27] C. L. Dezelah IV, J. Niinistö, K. Arstila, L. Niinistö, C. H. Winter, *Chem. Mater.* **2006**, *18*, 471.
[28] D. J. Comstock, J. W. Elam, *Chem. Mater.* **2012**, *24*, 4011.
[29] J. R. Waldrop, R. W. Grant, *Appl. Phys. Lett.* **1996**, *68*, 2879.
[30] S. W. Lee, Y. S. Lee, J. Heo, S. C. Siah, D. Chua, R. E. Brandt, S. B. Kim, J. P. Mailoa, T. Buonassisi, R. G. Gordon, *Adv. Energy Mater.* **2014**, 1301916.
[31] C. Malerba, F. Biccari, C. Leonor Azanza Ricardo, M. D'Incau, P. Scardi, A. Mittiga, *Sol. Energy Mater. Sol. Cells* **2011**, *95*, 2848.
[32] S. S. Wilson, Y. Tolstova, H. A. Atwater, *39th IEEE Photovoltaic Spec. Conf.*, DOI: 10.1109/PVSC.2013.6744960.
[33] J. Ghijsen, L. H. Tjeng, J. Vanelp, H. Eskes, J. Westerink, G. A. Sawatzky, M. T. Czyzyk, *Phys. Rev. B* **1988**, *38*, 11322.
[34] C. Xiang, G. M. Kimball, R. L. Grimm, B. S. Brunschwig, H. A. Atwater, N. S. Lewis, *Energy Environ. Sci.* **2011**, *4*, 1311.
[35] R. R. King, D. Bhusari, A. Boca, D. Larrabee, X. Q. Liu, W. Hong, C. M. Fetzer, D. C. Law, N. H. Karam, *Prog. Photovoltaics* **2011**, *19*, 797.
[36] L. C. Olsen, F. W. Addis, W. Miller, *Sol. Cells* **1982**, *7*, 247.
[37] M. Turcu, O. Pakma, U. Rau, *Appl. Phys. Lett.* **2002**, *80*, 2598.
[38] Y. S. Lee, M. T. Winkler, S. C. Siah, R. Brandt, T. Buonassisi, *Appl. Phys. Lett.* **2011**, *98*, 192115.
[39] Y. Liu, H. K. Turley, J. R. Tumbleston, E. T. Samulski, R. Lopez, *Appl. Phys. Lett.* **2011**, *98*, 162105.
[40] K. P. Musselman, Y. Ievskaya, J. L. MacManus-Driscoll, *Appl. Phys. Lett.* **2012**, *101*, 253503.
[41] Y. S. Lee, J. Heo, M. T. Winkler, S. C. Siah, S. B. Kim, R. G. Gordon, T. Buonassisi, *J. Mater. Chem. A* **2013**, *1*, 15416.